Cell Metabolism
Article

Chronic Sympathoexcitation through Loss of Vav3, a Rac1 Activator, Results in Divergent Effects on Metabolic Syndrome and Obesity Depending on Diet

Mauricio Menacho-Márquez,[1,2] Rubén Nogueiras,[3,4,5] Salvatore Fabbiano,[1,2,5] Vincent Sauzeau,[1,2,6] Omar Al-Massadi,[3,4] Carlos Diéguez,[3,4] and Xosé R. Bustelo[1,2,*]
[1]Centro de Investigación del Cáncer
[2]Instituto de Biología Molecular y Celular del Cáncer
Consejo Superior de Investigaciones Científicas (CSIC)-University of Salamanca, 37007 Salamanca, Spain
[3]Departamento de Fisioloxía
[4]Centro de Investigación en Medicina Molecular e Enfermidades Crónicas
University of Santiago de Compostela, 15782 Santiago de Compostela, Spain
[5]These authors contributed equally to this work
[6]Present address: L'Institut du Thorax, 44007 Nantes, France
*Correspondence: xbustelo@usal.es
http://dx.doi.org/10.1016/j.cmet.2013.07.001

SUMMARY

The role of the sympathetic nervous system, stress, and hypertension in metabolic syndrome and obesity remains unclear. To clarify this issue, we utilized genetically engineered mice showing chronic sympathoexcitation and hypertension due to lack of Vav3, a Rac1 activator. Here, we report that these animals develop metabolic syndrome under chow diet. However, they show protection from metabolic syndrome and obesity under fatty diets. These effects are elicited by α_1-adrenergic- and diet-dependent metabolic changes in liver and the α_1/β_3 adrenergic-mediated stimulation of brown adipocyte thermogenesis. These responses seem to be engaged by the local action of noradrenaline in target tissues rather than by long-range effects of adrenaline. By contrast, they are not triggered by low parasympathetic drive or the hypertensive state present in Vav3-deficient mice. These results indicate that the sympathetic system plays divergent roles in the etiology of metabolic diseases depending on food regimen, sympathoexcitation source, and disease stage.

INTRODUCTION

Metabolic syndrome (MS) encompasses a complex array of dysfunctions, such as type 2 diabetes, liver steatosis, dyslipemia, pan-inflammatory conditions, and hypertension, often, but not always, linked to obesity (Moller and Kaufman, 2005). This condition has become pandemic in recent years due to increased sedentary and high-calorie-diet lifestyles in both developing and industrialized societies (Hossain et al., 2007). It is therefore important to understand the physiological and metabolic mechanisms affecting the origin and progression of this complex disease.

One of the main mechanisms to buffer energy surpluses induced by high calorie intake is to engage energy-consuming anabolic and catabolic programs in the white adipose tissue (WAT) and brown adipose tissue (BAT), respectively. The WAT consumes energy by synthesizing and storing triglycerides. The BAT dissipates energy as heat using a thermogenic, mitochondrial-based program (Cannon and Nedergaard, 2004). These two activities are coordinated by the sympathetic nervous system (SNS) via the local release of noradrenaline (also known as norepinephrine) in WAT and BAT. This catecholamine promotes WAT lipolysis as well as BAT recruitment, lipolysis, and thermogenesis (Cannon and Nedergaard, 2004; Robidoux et al., 2004). In some conditions, the SNS can trigger further thermogenesis via the generation, expansion, and stimulation of brown-in-white (brite) adipocytes in the WAT (Robidoux et al., 2004). The SNS also controls basal metabolic rates and other diet-related processes (i.e., insulin secretion or glucose metabolism), thus ensuring the coordinated control of energy expenditure at the whole organism level (Lambert et al., 2010). Depending on the type of the physiological response involved, the SNS can regulate the above processes by releasing noradrenaline from local fibers or, alternatively, using the adrenaline (also known as epinephrine) secreted by the adrenal gland medulla (Lambert et al., 2010). The integration of metabolic parameters and SNS activation takes place primarily in different areas of the central nervous system that coordinate food intake and body weight. Those regions, in turn, receive signals from tissue afferents, adipose tissue-generated adipokines, thyroid hormones, and metabolites (Morton et al., 2006).

In addition to the disruption of adipose tissue-dependent responses during MS and obesity, it has been postulated that the development of some of those diseases can originate as a consequence of sustained activation of the SNS. In favor of this view, some epidemiological studies have shown that individuals affected by sympathetic-driven chronic stress, tachycardia, or borderline hypertension have higher tendencies to develop MS-related diseases and obesity (Lambert et al., 2010; Mancia et al., 2007; Pervanidou and Chrousos, 2012). Conversely, some studies have linked obesity-induced SNS activity with

increased tendencies to develop other comorbidities such as hypertension and atherosclerosis (Lambert et al., 2010; Mancia et al., 2007). However, it is worth noting the existence of quite a few contradictory clinical reports on all of those issues; so, at this moment, this is still an open area of debate (Lambert et al., 2010; Mancia et al., 2007).

To dissect the role of the SNS in MS ontogeny in a genetically clean manner, in this work we decided to use a knockout mouse strain for *Vav3*, a gene that encodes a Rho guanosine diphosphate (GDP)/guanosine triphosphate (GTP) exchange factor (Rho GEF) involved in the upstream activation of the Rac1 subfamily of Rho guanosine triphosphatases (GTPases) (Movilla and Bustelo, 1999). These animals display chronic sympathoexcitation due to axon migration and guidance defects that disrupt the GABAergic wiring that connects the caudal ventrolateral medulla (CVLM) with the rostral ventrolateral medulla (RVLM) in the brainstem. As a consequence, these animals develop RVLM- and SNS-associated dysfunctions such as tachycardia, tachypnea, hypertension, and other hypertension-related dysfunctions (Guyenet, 2006; Sauzeau et al., 2006, 2010a). Thus, we believed that this mutant mouse strain could represent an ideal tool to investigate the effect of sustained SNS hyperactivity and the VLM itself on both diet-induced physiological responses and the etiology of MS and obesity.

RESULTS

Vav3-Deficient Mice Develop Liver Steatosis and Type 2 Diabetes under Chow Diet Conditions

Given the general effects of the SNS on energy balance and basal metabolism (Lambert et al., 2010), we decided to investigate whether *Vav3*$^{-/-}$ mice had defects in any of those parameters under chow diet conditions. We did not find any difference between *Vav3*$^{-/-}$ and control mice in body weight (Figures S1A–S1C available online), percentages of fat and lean mass (Figures S1B and S1C), cumulative food intake (Figure S1D), circadian VO_2/VCO_2 quotients (Figure S1E), or overall energy expenditure (Figure S1F). These mice did show a slight reduction in locomotor activity during the dark period (Figure S1G). However, such difference was not relevant when normalized according to their specific lean mass (Figure S1G). In addition, no variations were observed in plasma levels of thyroid-stimulating hormone, triiodothyronine (T_3), or thyroxine (T_4) (Figures S1H–S1J).

Further analyses revealed that *Vav3*$^{-/-}$ mice developed hepatic steatosis, as evidenced by the abnormal large size (Figure 1A) and increased weight (Figure 1B) of livers obtained from euthanized animals. Consistent with this, we also observed the characteristic presence of lipid-enriched hepatocytes (Figures 1C and 1D) and high amounts of triglycerides (Figure 1E) in livers from *Vav3*$^{-/-}$ mice. The fatty liver disease became visually and histologically detectable in 4-month-old mice, and since then underwent a progressive worsening until reaching a nonalcoholic fatty liver or steatohepatitic state in ~90% of 1-year-old mice (Figures 1C and 1D). Alterations in liver function were indirectly confirmed by the detection of elevated concentrations of triglycerides (Figure 1F) and liver dysfunction markers such γ-glutamyl transpeptidase (GGT, Figure 1G) and bilirubin (Figure 1H) in the plasma of *Vav3*$^{-/-}$ mice. The hypertriglyceridemia coincided with the time in which the physical and histological signs of liver steatosis were detected (Figure 1F). However, GGT and bilirubin were already upregulated in 2-month-old mice (Figures 1G and 1H), indicating that liver dysfunctions started earlier than the physical manifestations of steatosis in *Vav3*$^{-/-}$ mice.

These mice also displayed typical signs of type 2 diabetes, including hyperglycemia (Figure 2A, compare values at time point 0), decreased glucose tolerance (Figures 2A and 2B), and hyperinsulinemia (Figures 2C and 2D). Impaired glucose tolerance was first detected in 2-month-old animals and remained a stable parameter throughout the life of Vav3-deficient mice (Figure 2B). The basal hyperinsulinemic state was also consistently detected in 3- to 12-month-old animals (Figure 2C). This last defect was due to both increased pancreatic secretion (Figure 2E) and reduced clearance by the liver (Figure 2F). The intravenous injection of insulin induced lower amounts of Akt phosphorylation in the liver (Figure 2G) and less efficient glucose clearance rates from circulation (Figure 2H) in *Vav3*$^{-/-}$ mice than in controls, further confirming the loss of Vav3-induced type 2 diabetes in mice. Quantitative RT-PCR (qRT-PCR) analyses indicated that these physiological changes correlated with progressive, time-dependent changes in the expression of transcripts associated with the development of a postreceptor insulin-resistant state (Figure S2A). The first change observed was the upregulation of the *Ppargc1a* messenger RNA (mRNA) in 1.5-month-old mice (Figures S2B and S2C). This transcript encodes Pgc1α, a cyclic AMP (cAMP)-induced transcriptional cofactor involved in glucagon-mediated fasting responses such as gluconeogenesis, fatty acid oxidation, and ketogenesis. It also favors insulin resistance by inhibiting Akt in a TRB3-dependent manner (Figure S2A) (Fernandez-Marcos and Auwerx, 2011). mRNAs for transcriptional factors involved in de novo lipogenesis and fatty liver disease (Srebp1, sterol regulatory element-binding protein 1) were first seen upregulated in 2.5-month-old mice (Figures S2A, S2C, and S2D) (Shao and Espenshade, 2012). By contrast, transcripts for Pparα and Insig2 became upregulated only in 3.5-month-old mice (Figures S2A–S2D). Pparα is a transcriptional factor that cooperates with Pgc1α in some signaling responses, including the induction of insulin resistance in a TRB3-dependent manner (Figure S2A) (Kersten et al., 2000). Insig2 is a negative regulator of Srebp1 that is positively and negatively regulated by Pparα and the insulin/phosphatidylinositol 3-kinase (PI3K)/Akt route, respectively (Figure S2A) (Dong and Tang, 2010). All those mRNAs were found upregulated in 6-month-old *Vav3*$^{-/-}$ mice (Figure S6). Despite this steatotic state, these mice did not develop typical peripheral dysfunctions associated with postreceptor insulin resistance, such as adipocyte hypertrophy or obesity (Figures S1B and S2C; see also Figure 3C) (Brown and Goldstein, 2008).

To rule out the possibility that this phenotype was induced by the hypertensive state of *Vav3*$^{-/-}$ mice, we performed similar analyses in mice deficient for a second member of the Vav family, Vav2. This mutant strain shows angiotensin II-dependent hypertension and high plasma catecholamine levels. However, unlike *Vav3*$^{-/-}$ mice, the upregulation of plasma catecholamines is angiotensin II dependent in this case and, therefore, is located downstream rather than upstream of the hypertensive condition (Sauzeau et al., 2010b). We did not find any sign of liver steatosis (Figures 2I and 2J), hyperinsulinemia (Figure 2K), hyperglycemia (Figure 2L), or impaired glucose tolerance (Figure 2L) in these

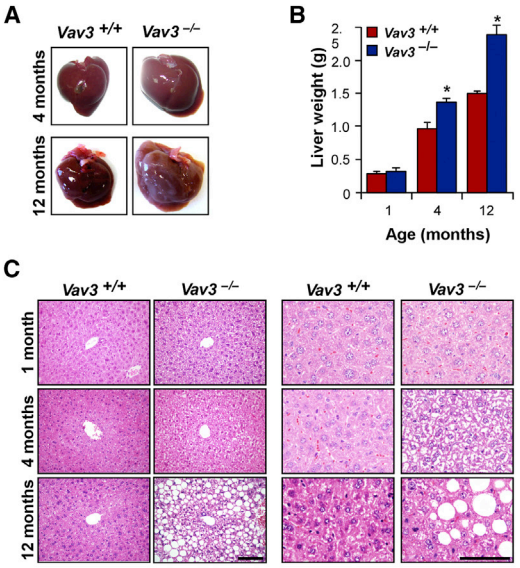

D

		Normal		NAFL		NASH
Age	Genotype	Stage 0	Stage 1	Stage 2	Stage 3	Stage 4
2 months	*Vav3* +/+	4/4 (100%)	0/4 (0%)	0/4 (0%)	0/4 (0%)	0/4 (0%)
	Vav3 −/−	3/5 (60%)	2/5 (10%)	0/5 (0%)	0/5 (0%)	0/5 (0%)
4 months	*Vav3* +/+	4/4 (100%)	0/4 (0%)	0/4 (0%)	0/4 (0%)	0/4 (0%)
	Vav3 −/−	0/12 (100%)	0/12 (0%)	3/12 (25%)	9/12 (75%)	0/12 (0%)
12 months	*Vav3* +/+	0/6 (100%)	2/6 (33%)	4/6 (66%)	0/6 (0%)	0/6 (0%)
	Vav3 −/−	0/7 (100%)	1/7 (14%)	0/7 (0%)	3/7 (43%)	3/7 (43%)

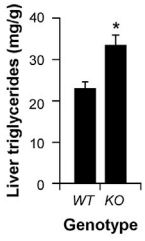

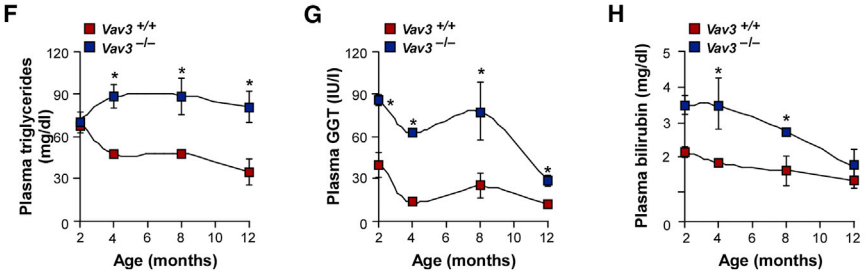

Figure 1. *Vav3*$^{-/-}$ Mice Develop Steatosis

(A and B) Representative images (A) and evolution of weight (B) of livers isolated from chow diet-fed mice of the indicated genotypes and ages. *p ≤ 0.05 relative to same-age controls (n = 5). In (A) and in the rest of the figures, all images of whole livers were taken using the same magnification.

(C) Representative images of histological sections obtained from livers of mice of indicated genotypes and ages. Scale bar = 100 μm.

(D) Anatomopathology of livers from mice of indicated genotypes and ages (left). The x/y ratio represents the number of animals (x) showing a given phenotype within the total number of animals (y) analyzed. Values diverging between control and mutant mice are shown in red. NAFL, nonalcoholic fatty liver; NASH, nonalcoholic steatohepatitis.

(E) Triglyceride content of livers from 4-month-old mice of indicated genotypes. *p ≤ 0.05 (n = 6). WT, wild-type mice; KO, *Vav3*$^{-/-}$ mice.

(F–H) Plasma concentrations of triglycerides (F), γ-glutamyl transpeptidase (GGT) (G), and bilirubin (H) in mice of the indicated genotypes and ages. *p ≤ 0.05 relative to values obtained at the same time point with controls (n = 4–5). Error bars in this figure represent the SEM. See also Figure S1.

mice, indicating that hypertension-mediated effects are not the direct cause of the MS present in *Vav3*$^{-/-}$ mice.

The Vav3 Deficiency Protects Mice from High-Fat-Diet-Induced Obesity

We next investigated whether the administration of a high-fat diet (HFD) could aggravate the fatty liver disease and insulin resistance of *Vav3*$^{-/-}$ mice. To that end, we fed cohorts of 2-month-old mice with a HFD for a 10-month-long period. Unlike wild-type animals, we observed that HFD-fed Vav3-deficient mice gained less weight (Figures 3A and S3A), had smaller fat deposits (Figures 3B and S3A), and did not develop white adipocyte hypertrophy (Figures 3C and 3D). Against our initial expectations, we also found that the HFD seemed to exert beneficial actions on *Vav3*$^{-/-}$ animals, since the abnormal increases in the weight and triglyceride content of livers previously found in chow diet-fed *Vav3*$^{-/-}$ mice were reduced by the HFD administration (Figures 3E–3H). Moreover, livers from HFD-fed mutant mice maintained the high abundance of the *Ppargc1a* mRNA but did not show the upregulation of *Srebp1c*, *Ppara*, or *Insig2* transcripts when compared to HFD-fed controls (Figure 3I). Consistent with the lack of steatosis, this tissue also showed a low abundance of the mRNA encoding fatty acid synthase (*Fasn*) (Figure 3I), an enzyme essential for lipid biosynthesis. HFD-fed *Vav3*$^{-/-}$ mice showed glucose tolerance (Figure 3J), insulin sensitivity (Figure 3K), and plasma insulin levels (Figure 3L) similar to those found in chow diet-fed wild-type mice, further indicating that the Vav3 deficiency affects obesity and MS-like dysfunctions in a diet-type-dependent manner.

Vav3-Deficient Mice Show Enhanced BAT Thermogenesis

The resistance to HFD-induced obesity of *Vav3*$^{-/-}$ mice was not due to changes in food intake (Figure S3B), circadian VO_2/VCO_2 quotients (Figure S3C), overall energy expenditure (Figures S3D and S3E), or the plasma concentration of the thyroid-derived T_3 (1.08 ± 0.06 versus 1.02 ± 0.08 ng/ml in controls) and T_4 (3.52 ± 0.19 versus 2.77 ± 0.26 ng/ml in controls; n = 5 mice/genotype) hormones. However, they showed increased levels of energy expenditure per lean mass (Figure S3E, right panel) and locomotor activity during the light period (Figure S3F). Further analyses indicated that they also displayed higher intrascapular surface (Figures 4A and 4B) and rectal (37.9°C ± 0.1°C versus

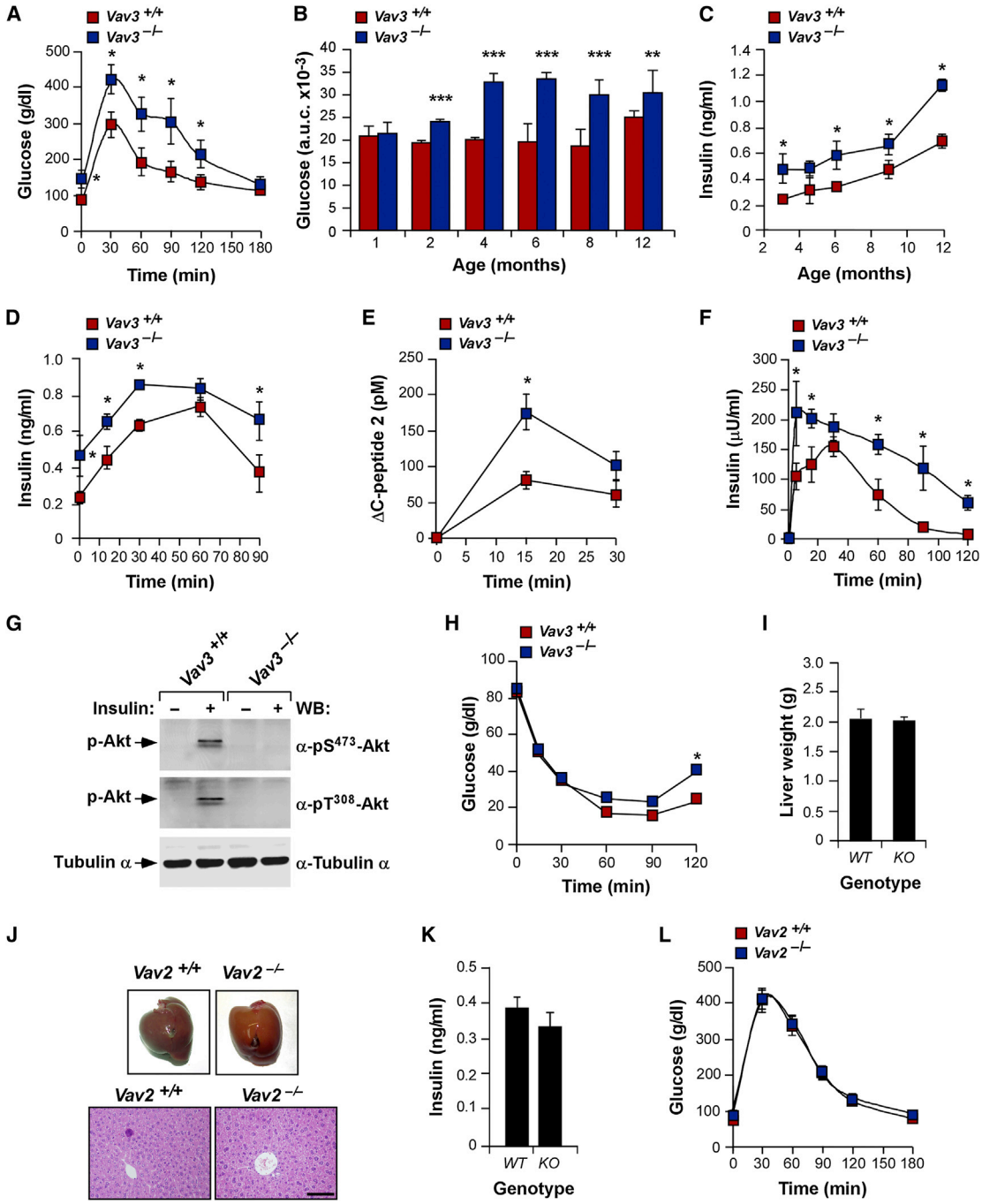

Figure 2. Chow-Fed *Vav3*$^{-/-}$ Mice Develop Type 2 Diabetes

(A) Glucose tolerance test showing reduced glucose tolerance in chow diet-fed 4-month-old *Vav3*$^{-/-}$ mice. *p ≤ 0.05 relative to values obtained at the same time point with controls (n = 5).

(B) Area under the curve (a.u.c.) values for the plasma concentration of glucose in mice of indicated genotypes and ages upon an injection of glucose. **p ≤ 0.01; ***p ≤ 0.001 relative to same-age controls (n = 5).

(C) Plasma insulin levels in mice of indicated genotypes and ages. *p ≤ 0.05 relative to values obtained at the same time point with controls (n = 4–6).

(D) Evolution of insulin plasma levels upon an injection of glucose in 4-month-old mice of indicated genotypes. *p ≤ 0.05 relative to values obtained at the same time point with controls (n = 3–4).

(E) Effect of glucose on insulin secretion (measured indirectly through the quantification of the plasma levels of the C-peptide proteolytic byproduct generated during insulin biosynthesis). *p ≤ 0.05 relative to values obtained at the same time point with controls (n = 4).

(F) Clearance rates of human insulin in control and *Vav3* null mice. *p ≤ 0.05 relative to values obtained at the same time point with controls (n = 3–4).

(G) Phosphorylation levels of Akt in indicated residues in the livers of mice of indicated genotypes that were either nontreated (–) or treated (+) with insulin. The expression of α-tubulin (bottom panel) was used as loading control.

(legend continued on next page)

37.1°C ± 0.2°C of controls; $p \leq 0.009$; n = 7) temperatures when compared to controls. This was associated to the activation of a BAT thermogenic program, as evidenced by the consistent, age-independent upregulation of the *Ucp1* mRNA in BAT samples from *Vav3*$^{-/-}$ mice (Figures 4C–4F). Ucp1 is a BAT-specific protein that uncouples oxidative phosphorylation from the respiratory chain, leading to energy dissipation as heat (Cannon and Nedergaard, 2004). The increase in the abundance of this transcript in both 2.5- and 3.5-month-old mice took place in parallel to the induction of Pgc1α (Figures 4E and 4F), the transcriptional factor involved in the transcriptional activation of the *Ucp1* gene during the thermogenic response (Cannon and Nedergaard, 2004). However, the *Ppargc1a* mRNA was not upregulated in the BAT of 0.5- and 1.5-month-old mice (Figures 4C and 4D), suggesting that other transcriptional factors were in charge of that role during those early postnatal periods. qRT-PCR analyses indicated that Krüppel-like factor 15 (Klf15) was the most likely candidate to functionally replace Pgc1α in the BAT of young mice (Figures S4A–S4D). Although the thermogenic response is usually associated with a decrease in fat vesicles present in brown adipocytes and a concomitant reduction in cell size, histological analyses revealed that the BAT from 1- and 6-month-old *Vav3*$^{-/-}$ mice was composed of cells harboring very large lipid vesicles that were more hypertrophic than those present in wild-type BAT samples (Figure 4G). As a result, we observed consistently lower cell densities in the BAT of *Vav3*$^{-/-}$ mice than in control animals in most ages tested (Figure 4H). This may reflect different differentiation degrees of brown adipocytes in control and mutant mice or, alternatively, that the lipolysis associated with the thermogenic program is compensated in standard diet-fed *Vav3*$^{-/-}$ mice by the uptake of lipids from other tissues such as the liver or WAT. This cytological pattern changed upon HFD administration. Thus, this diet induced the accumulation of large lipid vacuoles in brown adipocytes (Figure 4I) and a concomitant decrease in BAT cell density (Figure 4J) in the case of wild-type mice. By contrast, it promoted a reduction in lipid stores (Figure 4I) and an increase in BAT cell density (Figure 4J) in the case of *Vav3*$^{-/-}$ mice. Taken together, these observations indicate that the lack of obesity development in HFD-fed *Vav3*$^{-/-}$ mice is related to increased levels of both energy consumption per lean mass and BAT thermogenesis. This latter program is active even under standard diet and environmental temperature conditions.

Vav3-Deficient Mice Show Enhanced White-to-Brown Transdifferentiation

qRT-PCR analyses revealed that the *Ucp1* mRNA expression was also upregulated in WAT samples obtained from *Vav3*$^{-/-}$ mice (Figures S4E–S4I). Such an increase (8- to 9-fold) was in fact significantly higher than that seen in BAT of same animals (2- to 3-fold) (compare Figures 4C–4F and S4G–S4I). However, it developed at later times than in the case of BAT (compare Figures 4C–4F and S4E–S4I). Unlike the case of BAT, the WAT samples from *Vav3*$^{-/-}$ mice also displayed the parallel upregulation of *Ucp3* transcripts (Figures S4G and S4H). The transcripts for Pgc1α and some of its cotranscriptional partners (Pparα, Pparγ) were also elevated in WAT samples from 4.5-month-old *Vav3*$^{-/-}$ mice, but not in those from younger animals (Figures S4E–S4I), suggesting the implication of other transcriptional factors in the activation of the *Ucp1* gene in young *Vav3*$^{-/-}$ mice. Since *Ucp1* gene expression is limited to brown lineage cells (Cannon and Nedergaard, 2004), these results indicate the presence of ectopic thermogenesis in WAT via the generation and expansion of brite cells.

The Thermogenesis of Vav3-Deficient Mice Is Sympathetic Dependent

To investigate if the thermogenesis found in *Vav3*$^{-/-}$ mice was sympathetic dependent, we subjected control and mutant animals to treatments with a number of adrenergic antagonists. The administration of the SR59230A, a β_3 receptor inhibitor, promoted the rapid drop in the abundance of the *Ucp1* mRNA in the BAT of *Vav3*$^{-/-}$ mice that, under those conditions, reached values similar to those present in untreated control mice (Figure 5A). SR59230A had no effects on the abundance of the *Ucp1* transcript in the BAT of wild-type mice (Figure 5A). The administration of the generic β_1/β_2 adrenergic inhibitor propranolol did not have any effect in BAT *Ucp1* mRNA levels in *Vav3*$^{-/-}$ mice (Figure 5A). Doxazosin (an α_1 adrenergic receptor antagonist) promoted the short-term upregulation of the *Ucp1* mRNA content in the BAT of those mice (Figure 5A). In agreement with those results, we observed that the administration of SR59230A also eliminated the hyperthermia of *Vav3*$^{-/-}$ mice, whereas the same dose elicited no effect on the basal temperature of control animals (Figures 5B and 5C). These results indicate that chow diet-fed *Vav3*$^{-/-}$ mice activate BAT thermogenesis in a sympathetic-dependent manner and that such activation utilizes the classical prothermogenic noradrenaline/β_3 adrenergic receptor route present in brown and brite adipocytes.

Vav3$^{-/-}$ Mice Show Abnormal Regulation of SNS Activity during Both Chow and High-Fat Diet Conditions

We previously reported that the sympathoexcitation of *Vav3* null mice, measured indirectly as increased plasma levels of catecholamines, is detected in newborns and remains rather stable up to at least 1 year of age under standard chow diet conditions. This dysfunction precedes the angiotensin II-dependent hypertension and cardiovascular remodeling that takes place in these animals (Sauzeau et al., 2006). To investigate the evolution of SNS activity in HFD-fed animals, we periodically monitored the plasma concentration of those two catecholamines in mice subjected to a HFD since they were 2 months old. As control, we

(H) Evolution of the plasma concentration of glucose in 4-month-old mice of indicated genotypes upon an injection of insulin. *$p \leq 0.05$ relative to values obtained at the same time point with controls (n = 5).
(I) Liver weight of wild-type (WT) and *Vav2*$^{-/-}$ (KO) mice (n = 5).
(J) Representative images of livers (upper panels) and liver histological sections (lower panels) of mice from indicated genotypes.
(K) Plasma insulin levels in mice of indicated genotypes (n = 5).
(L) Evolution of the plasma concentration of glucose in mice of indicated genotypes during glucose tolerance tests (n = 5). All data shown in panels (I)–(L) were obtained using 4-month-old mice. Error bars in this figure represent the SEM. See also Figure S2.

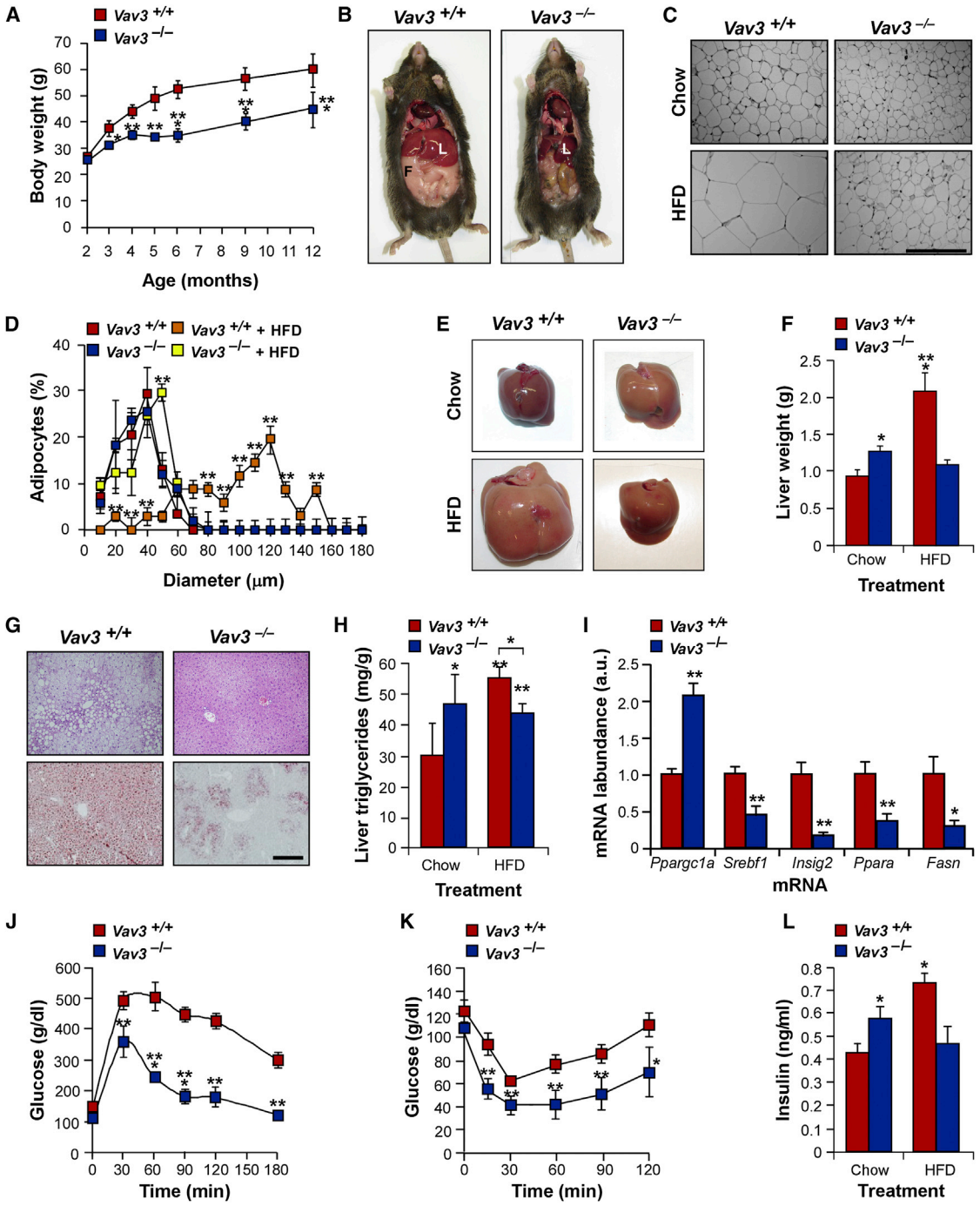

Figure 3. *Vav3*$^{-/-}$ Mice Are Resistant to Obesity and MS under HFD Conditions

(A) Evolution of body weight in animals of the indicated genotypes subjected to HFD since they were 2 months old. *p ≤ 0.05; **p ≤ 0.01; ***p ≤ 0.001 relative to values obtained at the same time point with controls (n = 5–6).

(B) Representative images of mice at the 6-month time point of the experiment shown in (A). F, fat; L, liver.

(C and D) Representative image of epigonadal WAT (C) and average size distribution of epigonadal white adipocytes (D) from 6-month-old mice of indicated genotypes that were kept under either chow or HFD conditions as in (A). **p ≤ 0.01 (n = 5).

(E and F) Representative image (E) and total weight (F) of livers extracted from 6-month-old mice of indicated genotypes previously kept under high-fat (HFD) or chow (Chow) diet conditions for 4 months. *p ≤ 0.05; ***p ≤ 0.001 relative to chow diet-fed controls (n = 5).

(G) Representative image of hematoxylin and eosin (H&E) (upper panels) and oil red O-stained (lower panels, to visualize lipids) liver sections from 6-month-old mice of indicated genotypes after being maintained under HFD conditions for 4 months. Scale bar = 200 μm.

(H) Triglyceride content of livers from 6-month-old mice of indicated genotypes after being fed under either chow or HFD conditions for 4 months. *p ≤ 0.05; **p ≤ 0.01 relative to chow diet-fed controls or indicated experimental pairs (in brackets) (n = 5).

(legend continued on next page)

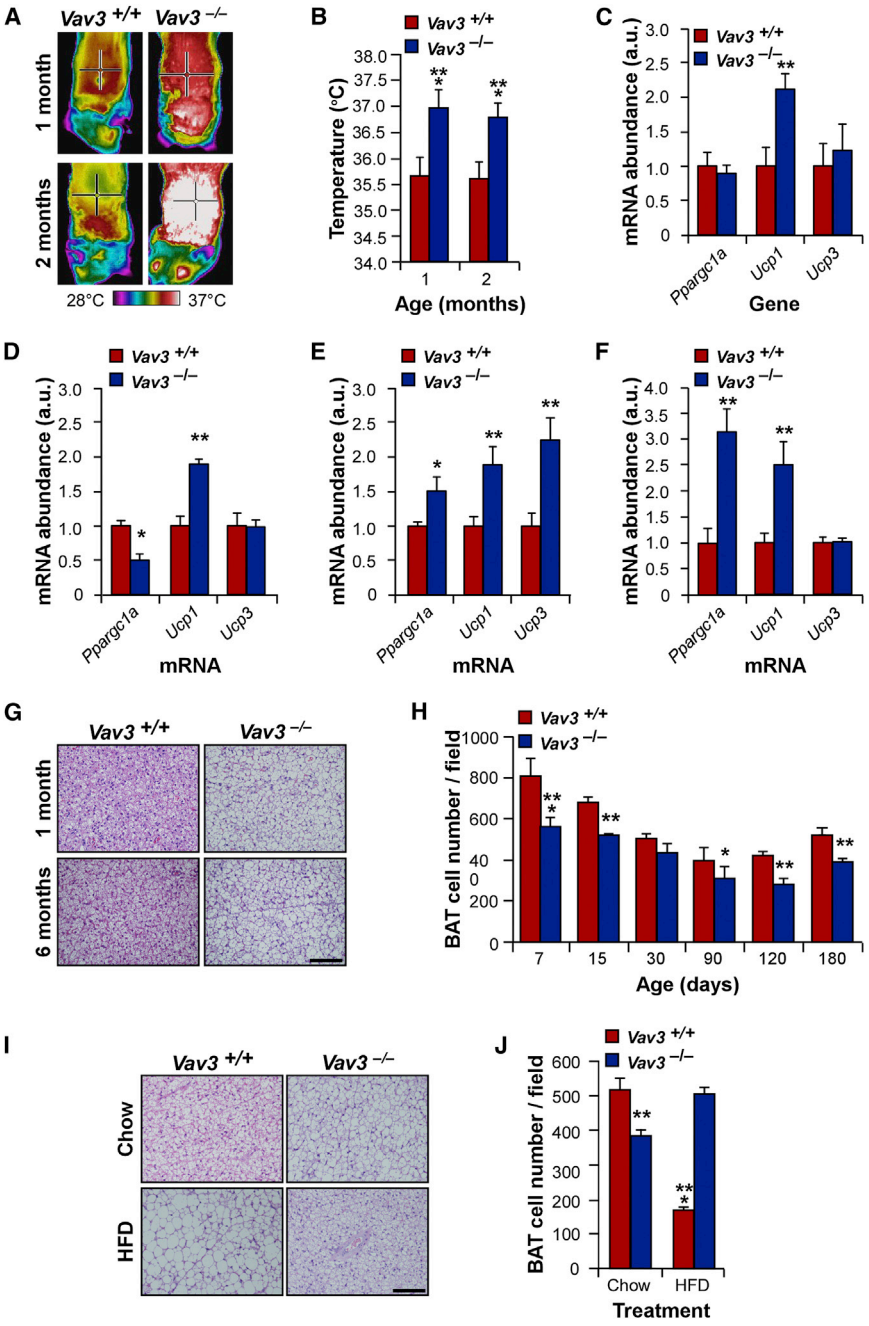

Figure 4. *Vav3*$^{-/-}$ Mice Show Enhanced BAT Thermogenesis

(A and B) Representative thermal images (A) and body temperature recordings (B) of chow diet-fed mice of indicated genotypes and ages. ***p ≤ 0.001 relative to same-age controls (n = 4–5).

(C–F) Abundance of indicated transcripts in the BAT of 0.5-month-old (C), 1.5-month-old (D), 2.5-month-old (E), and 3.5-month-old (F) wild-type and *Vav3*$^{-/-}$ mice maintained under chow diet conditions. Values obtained for each transcript in control mice were given an arbitrary value of 1. a.u., arbitrary units. *p ≤ 0.05; **p ≤ 0.01 (n = 3–4).

(G) Representative images of BAT sections from chow diet-fed mice of indicated genotypes and ages. Scale bar = 200 μm.

(H) Number of brown adipocytes present in intercapsular BAT sections from chow diet-fed mice of the same age. *p ≤ 0.05; **p ≤ 0.01; ***p ≤ 0.001 relative to same-age controls (n = 3–4).

(I) Representative images of BAT sections from 6-month-old mice of indicated genotypes after being fed a chow diet or HFD for 4 months. Scale bar = 200 μm.

(J) BAT cell density in animals from the experiment in (I). **p ≤ 0.01; ***p ≤ 0.001 relative to chow diet-fed controls (n = 3–4). Error bars in this figure represent the SEM. See also Figure S4.

maintained parallel groups of animals under chow diet. As expected (Sauzeau et al., 2006), *Vav3*$^{-/-}$ mice displayed higher plasma concentrations of noradrenaline (Figure 5D) and adrenaline (Figure 5E) than controls over the course of the experimental period under chow diet conditions. The HFD conditions had no influence on plasma noradrenaline during the first month of diet change in *Vav3*$^{-/-}$ mice but, since then, promoted a progressive reduction in the concentration of this catecholamine that, at the latest experimental time point, reached levels similar to those shown by chow diet-fed control mice (Figure 5D). HFD-fed wild-type mice displayed a transient, 3-fold increase in the plasma concentration of noradrenaline at 1 month into the diet change and, since that time point on, maintained higher amounts (2-fold) of plasma noradrenaline than when kept under chow diet (Figure 5E). The HFD conditions induced a further, although slight, increase of the plasma concentration of adrenaline in *Vav3*$^{-/-}$ mice upon the change into HFD (Figure 5E). However, unlike the case of noradrenaline, the plasma levels of adrenaline remained at high levels during the rest of the experiment conducted with Vav3-deficient mice (Figure 5E). The HFD promoted a progressive elevation of the plasma concentration of adrenaline in wild-type mice, with a maximum peak reached 4 months after the diet change (Figure 5E). These results indicate that the sympathoexcitation of *Vav3*$^{-/-}$ mice is present both in

(I) Abundance of indicated transcripts in the liver of HFD-fed control and mutant mice. *p ≤ 0.05; **p ≤ 0.01 (n = 5).

(J and K) Plasma concentration of glucose upon the injection of either glucose (J) or insulin (K) in 6-month-old wild-type and *Vav3*$^{-/-}$ mice previously subjected to HFD conditions during a 4-month period. *p ≤ 0.05; **p ≤ 0.01; ***p ≤ 0.001 relative to values obtained at the same time points with controls (n = 5).

(L) Plasma insulin levels present in overnight fasted 6-month-old mice of indicated genotypes and diet protocols. *p ≤ 0.05 relative to chow diet-fed controls (n = 5). Error bars in this figure represent the SEM. See also Figure S3.

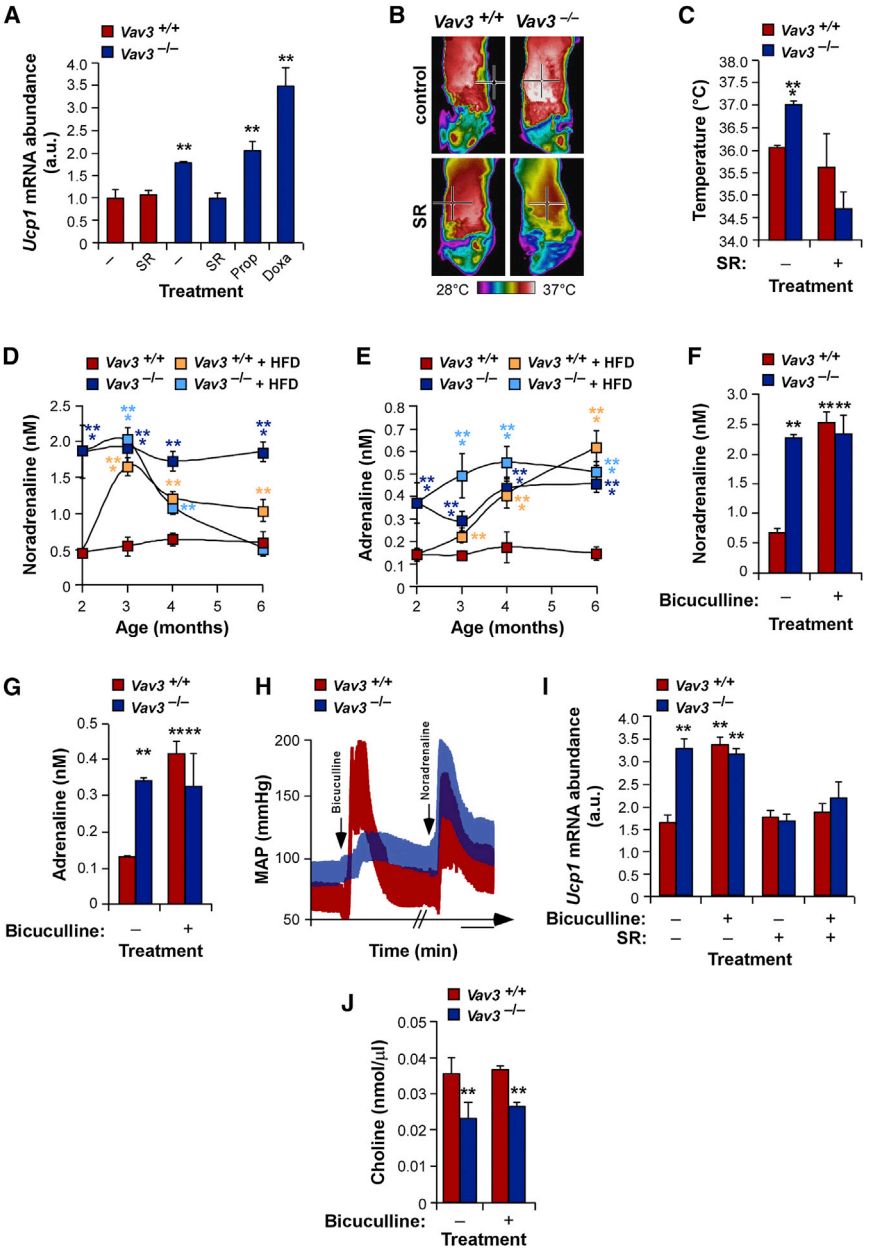

Figure 5. BAT Thermogenesis in *Vav3*$^{-/-}$ Mice Is Sympathetic Dependent

(A) Relative abundance of the *Ucp1* mRNA in the BAT of chow diet-fed animals of indicated genotypes that were either nontreated (–) or treated with the SR59230A (SR), propranolol (Prop), and doxazosin (Doxa) inhibitors. **p ≤ 0.01 (n = 5).

(B and C) Representative thermogram (B) and body temperatures (C) of chow diet-fed mice of indicated genotypes treated with either placebo (–) or SR59230A (+) for 24 hr. ***p ≤ 0.001 (n = 4).

(D and E) Plasma concentration of noradrenaline (D) and adrenaline (E) in chow and HFD-fed mice of indicated genotypes and ages. **p ≤ 0.01; ***p ≤ 0.001 relative to same-age controls (n = 5).

(F–J) Effect of bicuculline on the plasma concentrations of noradrenaline (F) and adrenaline (G), blood pressure (H), BAT *Ucp1* mRNA levels (I), and plasma choline (J) in chow diet-fed mice of indicated genotypes. In (H), animals were anesthetized and placed in blood pressure recording equipment. **p ≤ 0.01 (n = 5). Injection times are indicated by arrows. Scale bar = 1 min. Error bars in this figure represent the SEM. See also Figure S5.

chow diet and during early HFD periods. Furthermore, they show that the overall noradrenergic, but not the adrenergic, drive of these animals is inhibited upon the long-term administration of HFD.

Since the parasympathetic nervous system (PNS) plays roles in general metabolic regulation and liver glucose metabolism (Marino et al., 2011), we also analyzed the status of this branch of the autonomic system in both control and mutant mice. We observed that chow diet-fed *Vav3*$^{-/-}$ mice had a lower PNS tone, as evidenced by the lower plasma amount of choline, one of the degradation products of acetylcholine (Figure S5A). Consistent with this, we found that *Vav3*$^{-/-}$ mice also displayed delayed PNS-dependent gastrointestinal responses when compared to controls (Figures S5B and S5C). Similar results were found in *Vav2*$^{-/-}$ mice (Figure S5D), suggesting that the reduction of parasympathetic activity per se is not inextricably linked to the development of metabolic defects in mice. The overall PNS activity was reduced under HFD conditions in control and, to a much larger extent, in *Vav3*$^{-/-}$ mice (Figure S5E). This result rules out the possibility that the elimination of the MS-like phenotype in HFD-fed *Vav3*$^{-/-}$ mice could be due to a restoration or exacerbation of PNS tone. To further assess the potential contribution of lower PNS tone in the liver to the metabolic defects exhibited by *Vav3*$^{-/-}$ mice, we performed hepatic vagotomies to investigate the effects induced by the entire PNS denervation of liver on chow diet-fed wild-type mice. When compared to sham-operated mice, vagotomized mice exhibited normal parameters for overall autonomic activity (Figures S5F–S5H), cardiovascular and breathing rates (Figures S5I–S5K), liver structure (Figures S5L and S5M), plasma concentration of hepatic markers (Figures S5N–S5P), and glucose metabolism (Figures S5Q–S5S). Thus, in the absence of sympathoexcitation, the reduction of parasympathetic signals to the liver does not reproduce the dysfunctions seen in chow diet-fed *Vav3*$^{-/-}$ mice. Further analyses indicated that vagotomized mice did not have active thermogenic programs in the BAT (Figure S5T) and WAT (Figure S5U), ruling out the possibility that the activation of those processes in *Vav3*$^{-/-}$ mice could be indirectly derived from the elimination of vagally transmitted afferent signals from the liver.

The Thermogenesis and Hypertension of *Vav3*$^{-/-}$ Mice Show Similar Upstream, Sympathetic-Dependent Coregulation

We have previously shown that the stereotaxic administration of a $GABA_A$ receptor antagonist (bicuculline) into the RVLM of wild-type mice phenocopies the *Vav3* gene deficiency in terms of induction of high plasma catecholamine levels, tachypnea, tachycardia, and hypertension in mice. By contrast, this drug has a minor impact on *Vav3*$^{-/-}$ mice since they have already lost the tonic inhibitory control regulated by presynaptic GABAergic neurons present in the RVLM (Sauzeau et al., 2010a). During these experiments, we observed that bicuculline induced the same aforementioned effects when administered intravenously at low doses to mice. We used this strategy to investigate whether the hyperthermia and hypertension were subjected to similar upstream controls by the SNS in chow diet-fed *Vav3*$^{-/-}$ mice. We found that bicuculline induced a sharp and rapid elevation of plasma catecholamines (Figures 5F and 5G), blood pressure (Figure 5H), and BAT *Ucp1* mRNA levels (Figure 5I) when administered to wild-type mice. The latter effect could be blocked by the SR59230A β_3 receptor antagonist, further confirming that bicuculline induced the *Ucp1* transcript in wild-type brown adipocytes in a noradrenaline/β_3 receptor-dependent manner (Figure 5I). However, and similar to the marginal effect on the elevation of both plasma catecholamine (Figures 5F and 5G) and blood pressure levels (Figure 5H), bicuculline had no detectable impact on the abundance of the BAT *Ucp1* transcript when injected into *Vav3*$^{-/-}$ mice (Figure 5I). As a control, the administration of noradrenaline induced similar increases in blood pressure in wild-type and *Vav3*$^{-/-}$ mice (Figure 5H). The administration of bicuculline had no effect on the plasma levels of choline in both wild-type and mutant mice (Figure 5J), indicating that the short-term systemic administration of this drug only had an effect in the sympathetic branch of the autonomic nervous system. These results indicate that the hypertension and BAT hyperthermia present in *Vav3*$^{-/-}$ mice are both associated to dysfunctions in the tonic control of the SNS by inhibitory GABAergic signals.

α_1 Adrenergic Receptor Antagonists Block the Metabolic Dysfunctions Present in Chow- and HFD-fed *Vav3*$^{-/-}$ Mice

The results presented in the previous sections did not give any hint about the potential implication of the SNS in the liver steatosis and type 2 diabetes exhibited by *Vav3*$^{-/-}$ mice under chow diet conditions. To tackle this issue, we decided to investigate the effect of the systemic administration of α_1 (doxazosin) and β_1/β_2 (propranolol) adrenergic receptor antagonists in chow diet-fed *Vav3*$^{-/-}$ and wild-type mice. We chose those inhibitors because α_1 and β_2 adrenergic receptors play major roles in metabolic regulation in liver, skeletal muscle, and other tissues, including brain (Lambert et al., 2010). To that end, we started the administration of adrenergic receptor antagonists in chow diet-fed 1-month-old animals and evaluated the results 5 months later under the same diet conditions (Figure 6A). To get further information about the effect of adrenergic receptor inhibitors on the metabolic phenotype of *Vav3*$^{-/-}$ mice, we also decided to monitor the effect of such treatments on animals that were fed under HFD for the last 4 months of the experiment (Figure 6A).

We found that the long-term application of either doxazosin or propranolol had no effects on the overall weight (Figure 6B) and WAT content (data now shown) of chow diet-fed *Vav3*$^{-/-}$ mice. However, doxazosin, but not propranolol, prevented the development of hepatic steatosis in chow diet-fed mutant mice, as demonstrated by the wild-type-like size (Figures 6C and 6D), histology (Figure 6E), and triglyceride content (Figure 6F) of their livers (for a summary of these results, see Figure S6A). Interestingly, these treatments differentially affected the transcripts previously found upregulated in the liver of *Vav3*$^{-/-}$ mice. Thus, doxazosin eliminated the upregulation of *Ppargc1a*, *Srebp1a*, and *Srebp1c* mRNAs (Figure S6B), whereas propranolol only affected the expression of the *Ppargc1a* transcript (Figure S6B). The overexpression of *Insig2* and *Ppara* mRNAs was not eliminated by any of those drugs (Figure S6B), suggesting that they were not regulated by SNS signals. Consistent with the acquisition of normal metabolic responses, we observed that the long-term doxazosin treatment blocked the development of the hyperinsulemic (Figure 6G) and the glucose intolerance (Figure 6H) states present in *Vav3*$^{-/-}$ mice (Figure S6A). Unlike in the case of the short-term experiments (Figure S5A), doxazosin also eliminated the thermogenic program previously observed in the BAT, as demonstrated by the reduced abundance of *Ppargc1a* and *Ucp1* mRNAs in the BAT of *Vav3*$^{-/-}$ mice (Figures S6C and S6D). Propranolol treatments did not eliminate any of those dysfunctions (Figures 6G, 6H, S6A, and S6C).

Under HFD conditions, doxazosin abrogated the protective effect of the Vav3 deficiency on weight gain (Figure 6B), WAT expansion (Figure 6I), white adipocyte hyperplasia (Figure 6J), obesity-induced liver steatosis (Figures 6C–6E), and obesity-triggered glucose intolerance (Figures 6H and S6A). It also eliminated the thermogenic programs in the BAT (Figures 6K and S6D) and WAT (Figure S6E) of *Vav3*$^{-/-}$ mice. These results indicate that the chronic stimulation of α_1 adrenergic receptors contributes to the development of MS in chow-fed *Vav3*$^{-/-}$ mice and, in combination with β_3 adrenergic receptors, to the anti-obesity and anti-MS effects of the Vav3 deficiency in HFD-fed mice (Figures S6A and S6F). By contrast, β_1/β_2 adrenergic receptor-dependent mechanisms did not seem to contribute to any of the above processes, since parallel propranolol treatments did not induce any detectable effect on the metabolic phenotype of both chow and HFD-fed *Vav3*$^{-/-}$ mice (Figures S6A and S6F).

DISCUSSION

This work has revealed that chow diet-fed *Vav3*$^{-/-}$ mice develop an incomplete postreceptor insulin state characterized by typical liver and plasma MS-like pathophysiologies that, unexpectedly, is not associated to other defects such as white adipocyte hypertrophy and obesity (Brown and Goldstein, 2008). Interestingly, these mice do not develop those dysfunctions when maintained under long-term HFD conditions and, in addition, show a marked protection from the obesity and MS usually elicited by that food regimen. Our results indicate that several SNS-dependent processes contribute to the development of this metabolic phenotype. The lack of increased adiposity and obesity observed in these animals under both diet conditions

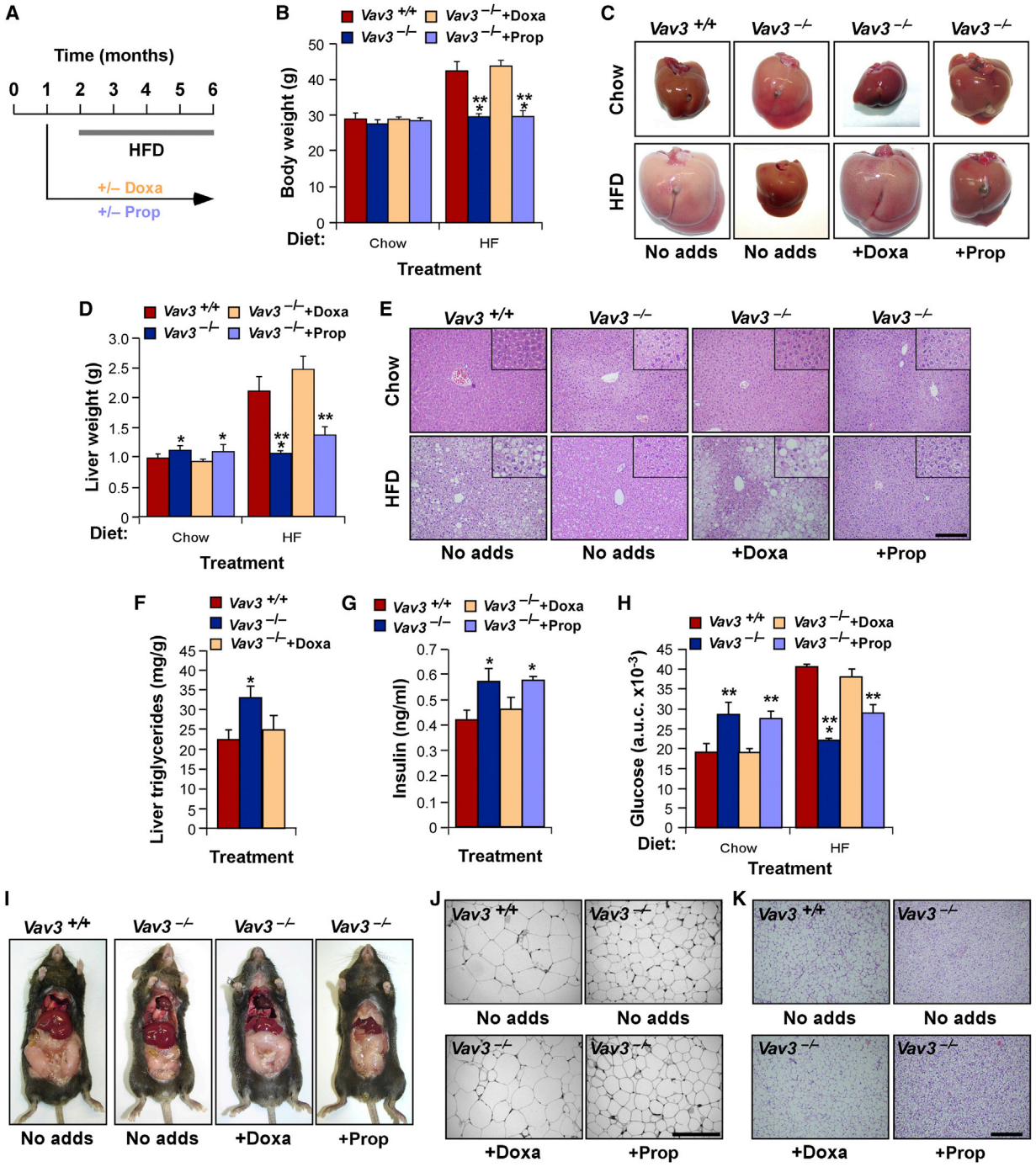

Figure 6. α_1 Adrenergic Receptor Antagonists Block the Metabolic Dysfunctions Present in Chow- and HFD-Fed *Vav3*$^{-/-}$ Mice

(A) Scheme of these experiments.

(B–F) Effect of doxazosin (Doxa) and propranolol (Prop) on total body weight (B) as well as on the appearance (C), overall weight (D), histology (E), and triglyceride content (F) of livers of *Vav3*$^{-/-}$ mice fed under chow or HFD (HF) conditions. *p $\leq$ 0.05; **p $\leq$ 0.01; ***p $\leq$ 0.001 relative to controls under the same diet type (n = 5). Scale bar in (E) = 200 μm.

(G) Plasma levels of insulin in 6-month-old mice fasted overnight and subjected to chow diet and treatments with adrenergic receptor antagonists as above. *p $\leq$ 0.05 (n = 5).

(H) a.u.c. values of the plasma concentration of glucose in 6-month-old mice of indicated genotypes and treatments upon using a glucose tolerance test. **p $\leq$ 0.01; ***p $\leq$ 0.001 relative to controls under the same diet type (n = 5).

(I) Representative images of HFD-fed 6-month-old mice of indicated genotypes and treatments.

(J and K) Histological epigonadal WAT (J) and scapular BAT (K) sections from HFD-fed 6-month-old mice of indicated genotypes and treatments. Scale bar = 200 μm. Error bars in this figure represent the SEM. See also Figure S6.

can be explained by the SNS-mediated activation of thermogenic programs in the BAT and, subsequently, in WAT. Notably, these programs are activated independently of the dietary (HFD) or environmental (i.e., cold exposure) conditions that normally trigger them under physiological conditions. The cause of the diet-dependent diabetes and steatosis of these animals remains to be fully explained from a mechanistic point of view. However, an integrated analysis of the pathophysiological and molecular changes exhibited by these mice suggests that it may entail both liver-autonomous (diet-independent) and nonautonomous (diet-dependent) alterations. Consistent with the presence of intrinsic signaling events in the liver, we have observed that the SNS-dependent upregulation of the *Ppargc1a* mRNA in this tissue takes place independently of the diet type and pathophysiological status of *Vav3*$^{-/-}$ mice (Figure S6F). By contrast, the expression of the *Srebp1*, *Ppara*, and *Insig2* mRNAs is highly dependent on the diet type and presence of active thermogenic programs (Figure S6F). The regulation of these transcripts is also heterogeneous, since their expression is SNS dependent (*Srebp1*) and independent (*Ppara*, *Insig2*) (Figure 6F). These results indicate that this latter expression program is controlled by signaling events extrinsic to the liver. The WAT and BAT are likely candidates to trigger those nonautonomous responses, as evidenced by the correlation observed between the doxazosin-mediated inactivation of thermogenic programs in those tissues and the elimination of the protection offered by the Vav3 deficiency against HFD-induced obesity and MS (Figure S6A). Given the drastic antidiabetic and steatotic effects induced by minor variations in the activity of lipolytic and fatty acid oxidation routes in adipocytes (Girousse et al., 2013; Waki et al., 2007), it is possible that such influence could be mediated by diet-dependent changes in the flux of free fatty acids and triglycerides between them and the liver. Consistent with this, we have observed significant changes in the histology and abundance of *Pargc1a* and *Ucp1* mRNAs in the BAT, depending on the diet type (Figures 4 and S6D). Other possibilities include HFD-dependent changes in adrenergic drive among different tissues and/or the activation of neuroendocrine afferent- or efferent-based loops affecting liver metabolic output. More work will be required to fully understand this process.

We have shown that *Vav3*$^{-/-}$ mice develop SNS-dependent dysfunctions due to the loss of tonic GABAergic inhibitory control of the RVLM (Sauzeau et al., 2010a; Sauzeau et al., 2006). It is possible, therefore, that the metabolic defects reported here could have a similar etiology. The lack of feeding or thyroid hormone alterations in *Vav3*$^{-/-}$ mice also argues against a direct implication of sympathoregulatory areas of the brain associated to food intake and energy expenditure in this phenotype (Morton et al., 2006). However, it is worth noting that the BAT thermogenesis found in *Vav3*$^{-/-}$ mice is at odds with the known inhibitory effects of the RVLM in this process (Madden, 2012; Morrison, 1999). This discrepancy can be taken as evidence for the presence of additional dysfunctions in other thermoregulatory centers in these mice, such as the rostral raphe pallidus (rRPa) (Morrison et al., 2008). Alternatively, it is possible that the disinhibited RVLM of *Vav3*$^{-/-}$ mice could induce rRPa-independent thermogenesis through the chronic stimulation of sympathetic fibers that innervate the intra-BAT vasculature. This is in agreement with observations showing that, under normothermia conditions, local sympathetic activity in the BAT correlates well with the activity level of RVLM-regulated functions such as heart rate and blood pressure (Morrison, 1999). A similar explanation can be used for the stimulation of WAT thermogenesis and liver routes, since most of the catecholaminergic nerve terminals in these tissues are adjacent to blood vessels (Robidoux et al., 2004; Yi et al., 2010). In any case, and given the multiple sympathoregulatory areas involved in metabolic regulation, we cannot formally exclude the possibility that the Vav3 deficiency could affect some of those areas in either RVLM-dependent or -independent fashions. If that were the case, our bicuculline experiments suggest that such a role must still be linked to the proper wiring of inhibitory, GABAergic-dependent signals. In the same context, is also possible that SNS-dependent metabolic defects could be further accentuated by the parallel reduction in PNS tone present in *Vav3*$^{-/-}$ mice.

The increased levels of catecholamines in the plasma of *Vav3*$^{-/-}$ mice also raise the issue of whether their metabolic defects are induced through sympathetic efferents (using either direct innervations or local paracrine actions from catecholamine spillover) and/or long-range, adrenaline-mediated signals. We currently favor the former possibility, since *Vav2*$^{-/-}$ mice show no metabolic defects, despite displaying similar levels of plasma catecholamines (Sauzeau et al., 2007). Likewise, knockin mice lacking Rac1 expression exclusively in vascular smooth muscle cells indicate that they do not develop diabetes or steatosis, despite displaying a *Vav2*$^{-/-}$ cardiovascular phenotype and elevated, angiotensin II-induced plasma levels of catecholamines (S.F., M.M.-M., and X.R.B., unpublished data). We have also observed that the chronic infusion of catecholamines in wild-type mice for 15 days using implanted drug-delivery pumps does not trigger the upregulation of the *Ppargc1a* mRNA in liver (data not shown). Notwithstanding this evidence, it is quite possible that a hormonal-based mechanism could participate in other metabolic programs not explored in this work. For example, it is known that the RVLM reacts to glycoprivation by stimulating adrenaline secretion from the adrenal gland (Verberne and Sartor, 2010). Further analyses of additional SNS-regulated metabolic responses will be important to identify the spectrum of pathophysiological defects present in these mice and the nervous and hormonal mechanisms involved in triggering them.

There is a lot of debate regarding the implication of chronic sympathoexcitation and stress in the development of MS and obesity and whether hypertension can favor insulin resistance and MS. There are also conflicting reports on whether the obesity-induced SNS activity can drive or collaborate in the development of associated diseases such as hypertension or atherosclerosis (Lambert et al., 2010; Mancia et al., 2007; Pervanidou and Chrousos, 2012). Solving these issues is important to understanding whether those diseases are etiologically intertwined or, alternatively, whether they codevelop independently in patients due to either dietary habits or lifestyle. However, it has been rather difficult answering them at the clinical level given the multiple ethnic, gender, and environmental factors influencing the evolution of those diseases in humans (Lambert et al., 2010). The sympathoexcitation present in Vav family knockout mice has given us the opportunity to address some of those questions in a genetically and environmentally "clean" manner. Our results are consistent with the idea that

chronic sympathoexcitation does promote the development of pathophysiological dysfunctions traditionally linked to MS. In this context, they also suggest that treatments with doxazosin, but not with β_1/β_2 blockers such as propranolol, could be beneficial to eliminate MS-related dysfunctions in the case of nonobese individuals with both MS and signs of high SNS activity (i.e., hypertension, tachycardia). Such a benefit would represent a burden, however, in the case of obese individuals with increased SNS activity, since doxazosin would block the protective effect of chronic sympathoexcitation on obesity and obesity-induced MS. By contrast, our data are not consistent with an implication of chronic sympathoexcitation in the development of obesity regardless of the diet type used. Our work also rules out any direct effects of hypertension per se on insulin resistance at the systemic level, because *Vav2*$^{-/-}$ mice do not display any overt signs of insulin resistance or steatosis, despite exhibiting angiotensin II-dependent hypertension (Sauzeau et al., 2007). The results obtained with wild-type mice do support the generally held idea that obesity does promote SNS activation. However, the examination of that response during a 10-month-long period has revealed that such regulation is highly complex, since it involves the differential and time-dependent regulation of both sympathetic neurons and the adrenal gland medulla.

These results have unveiled the implication of a Rho GEF in biological programs connected to the regulation of metabolic diseases. However, our genome encodes more than 60 additional Rho GEFs (Bos et al., 2007), many of which are expressed in tissues involved in metabolic regulation, such as the liver, adipose tissue, muscle, or brain. It is therefore quite important to conduct further genetic analyses with members or this enzyme family to identify new therapeutically appealing targets for the treatment of MS, obesity, and associated diseases.

EXPERIMENTAL PROCEDURES

Animal Studies

Vav3$^{-/-}$ and *Vav2*$^{-/-}$ C57BL/10 mice (Doody et al., 2001; Sauzeau et al., 2006) were utilized according to protocols approved by the Bioethics Committees of the University of Salamanca, CSIC, and the University of Santiago de Compostela. Mice were kept in ventilated rooms in pathogen-free facilities under controlled temperature (23°C), humidity (50%), and illumination (12 hr light/12 hr dark cycle) conditions. After weaning, mice were fed a standard chow global diet #2918 (6.2% fat, 3.1 kcal/g; Harlan Laboratories). When indicated, 2-month-old mice were shifted to a HFD protocol (45% fat, 4.73 kcal/g; Research Diets). Experimental procedures involving these mice are described in the Supplemental Experimental Procedures.

Statistics

Data were analyzed using one-way ANOVA or Student's t test for comparison between two unpaired groups. Values were considered significant when $p \leq 0.05$. In all figures, data values are given as mean ± SEM.

SUPPLEMENTAL INFORMATION

Supplemental Information includes Supplemental Experimental Procedures and six figures and can be found with this article online at http://dx.doi.org/10.1016/j.cmet.2013.07.001.

ACKNOWLEDGMENTS

We thank J.M. López-Novoa for comments on this work and A. Abad, M. Blázquez, and T. Teixeira for technical assistance. Work was supported by grants from the Spanish Ministry of Economy & Competitiveness to X.R.B. (SAF2009-07172, SAF2012-31371, RD06/0020/0001, RD12/0036/0002), R.N. (RYC-2008-02219, SAF2009-07049), and C.D. (BFU2011, CIBER de Fisiopatología de la Obesidad y Nutrición); the Galician Autonomous Government to R.N. (2010/14); and the European Union 7th Framework Program to R.N. (ERC-2011-StG-OBESITY53-281408, 245009) and C.D. (245009). Spanish funding was cosponsored by the European Regional Development Fund. The authors declare no competing financial interests.

M.M.-M. carried out the work regarding Figures 1, 2, 3, 4, 5, 6, S1, S2, and S4–S6. R.N. and C.D. carried out work shown in Figures 2, 3, 4, 5, S1, S3, and S5. S.F. worked on Figures 2, 3, 4, 5, 6, S5, and S6. V.S. carried out work related to Figures 1, 2, 5, and S3. O.A.-M. performed hepatic vagotomies. X.R.B. designed the work, wrote the manuscript, and carried out the final figure editing.

Received: December 18, 2012
Revised: May 27, 2013
Accepted: July 3, 2013
Published: August 6, 2013

REFERENCES

Bos, J.L., Rehmann, H., and Wittinghofer, A. (2007). GEFs and GAPs: critical elements in the control of small G proteins. Cell *129*, 865–877.

Brown, M.S., and Goldstein, J.L. (2008). Selective versus total insulin resistance: a pathogenic paradox. Cell Metab. *7*, 95–96.

Cannon, B., and Nedergaard, J. (2004). Brown adipose tissue: function and physiological significance. Physiol. Rev. *84*, 277–359.

Dong, X.Y., and Tang, S.Q. (2010). Insulin-induced gene: a new regulator in lipid metabolism. Peptides *31*, 2145–2150.

Doody, G.M., Bell, S.E., Vigorito, E., Clayton, E., McAdam, S., Tooze, R., Fernandez, C., Lee, I.J., and Turner, M. (2001). Signal transduction through Vav-2 participates in humoral immune responses and B cell maturation. Nat. Immunol. *2*, 542–547.

Fernandez-Marcos, P.J., and Auwerx, J. (2011). Regulation of PGC-1α, a nodal regulator of mitochondrial biogenesis. Am. J. Clin. Nutr. *93*, 884S–90.

Girousse, A., Tavernier, G., Valle, C., Moro, C., Mejhert, N., Dinel, A.L., Houssier, M., Roussel, B., Besse-Patin, A., Combes, M., et al. (2013). Partial inhibition of adipose tissue lipolysis improves glucose metabolism and insulin sensitivity without alteration of fat mass. PLoS Biol. *11*, e1001485.

Guyenet, P.G. (2006). The sympathetic control of blood pressure. Nat. Rev. Neurosci. *7*, 335–346.

Hossain, P., Kawar, B., and El Nahas, M. (2007). Obesity and diabetes in the developing world—a growing challenge. N. Engl. J. Med. *356*, 213–215.

Kersten, S., Desvergne, B., and Wahli, W. (2000). Roles of PPARs in health and disease. Nature *405*, 421–424.

Lambert, G.W., Straznicky, N.E., Lambert, E.A., Dixon, J.B., and Schlaich, M.P. (2010). Sympathetic nervous activation in obesity and the metabolic syndrome—causes, consequences and therapeutic implications. Pharmacol. Ther. *126*, 159–172.

Madden, C.J. (2012). Glucoprivation in the ventrolateral medulla decreases brown adipose tissue sympathetic nerve activity by decreasing the activity of neurons in raphe pallidus. Am. J. Physiol. Regul. Integr. Comp. Physiol. *302*, R224–R232. Published online November 9, 2011. http://dx.doi.org/10.1152/ajpregu.00449.2011.

Mancia, G., Bousquet, P., Elghozi, J.L., Esler, M., Grassi, G., Julius, S., Reid, J., and Van Zwieten, P.A. (2007). The sympathetic nervous system and the metabolic syndrome. J. Hypertens. *25*, 909–920.

Marino, J.S., Xu, Y., and Hill, J.W. (2011). Central insulin and leptin-mediated autonomic control of glucose homeostasis. Trends Endocrinol. Metab. *22*, 275–285.

Moller, D.E., and Kaufman, K.D. (2005). Metabolic syndrome: a clinical and molecular perspective. Annu. Rev. Med. *56*, 45–62.

Morrison, S.F. (1999). RVLM and raphe differentially regulate sympathetic outflows to splanchnic and brown adipose tissue. Am. J. Physiol. *276*, R962–R973.

Morrison, S.F., Nakamura, K., and Madden, C.J. (2008). Central control of thermogenesis in mammals. Exp. Physiol. *93*, 773–797.

Morton, G.J., Cummings, D.E., Baskin, D.G., Barsh, G.S., and Schwartz, M.W. (2006). Central nervous system control of food intake and body weight. Nature *443*, 289–295.

Movilla, N., and Bustelo, X.R. (1999). Biological and regulatory properties of Vav-3, a new member of the Vav family of oncoproteins. Mol. Cell. Biol. *19*, 7870–7885.

Pervanidou, P., and Chrousos, G.P. (2012). Metabolic consequences of stress during childhood and adolescence. Metabolism *61*, 611–619.

Robidoux, J., Martin, T.L., and Collins, S. (2004). Beta-adrenergic receptors and regulation of energy expenditure: a family affair. Annu. Rev. Pharmacol. Toxicol. *44*, 297–323.

Sauzeau, V., Sevilla, M.A., Rivas-Elena, J.V., de Alava, E., Montero, M.J., López-Novoa, J.M., and Bustelo, X.R. (2006). Vav3 proto-oncogene deficiency leads to sympathetic hyperactivity and cardiovascular dysfunction. Nat. Med. *12*, 841–845.

Sauzeau, V., Jerkic, M., López-Novoa, J.M., and Bustelo, X.R. (2007). Loss of Vav2 proto-oncogene causes tachycardia and cardiovascular disease in mice. Mol. Biol. Cell *18*, 943–952.

Sauzeau, V., Horta-Junior, J.A.C., Riolobos, A.S., Fernández, G., Sevilla, M.A., López, D.E., Montero, M.J., Rico, B., and Bustelo, X.R. (2010a). Vav3 is involved in GABAergic axon guidance events important for the proper function of brainstem neurons controlling cardiovascular, respiratory, and renal parameters. Mol. Biol. Cell *21*, 4251–4263.

Sauzeau, V., Sevilla, M.A., Montero, M.J., and Bustelo, X.R. (2010b). The Rho/Rac exchange factor Vav2 controls nitric oxide-dependent responses in mouse vascular smooth muscle cells. J. Clin. Invest. *120*, 315–330.

Shao, W., and Espenshade, P.J. (2012). Expanding roles for SREBP in metabolism. Cell Metab. *16*, 414–419.

Verberne, A.J., and Sartor, D.M. (2010). Rostroventrolateral medullary neurons modulate glucose homeostasis in the rat. Am. J. Physiol. Endocrinol. Metab. *299*, E802–E807.

Waki, H., Park, K.W., Mitro, N., Pei, L., Damoiseaux, R., Wilpitz, D.C., Reue, K., Saez, E., and Tontonoz, P. (2007). The small molecule harmine is an antidiabetic cell-type-specific regulator of PPARgamma expression. Cell Metab. *5*, 357–370.

Yi, C.X., la Fleur, S.E., Fliers, E., and Kalsbeek, A. (2010). The role of the autonomic nervous liver innervation in the control of energy metabolism. Biochim. Biophys. Acta *1802*, 416–431.